Shaan Bibi Jaffri and Khuram Shahzad Ahmad*

Foliar-mediated Ag:ZnO nanophotocatalysts: green synthesis, characterization, pollutants degradation, and *in vitro* biocidal activity

https://doi.org/10.1515/gps-2018-0058
Received March 5, 2018; accepted July 20, 2018; previously published online September 4, 2018

Abstract: A green, biomimetic, and one-pot synthesis of silver-doped zinc oxide (ZnO:Ag) nanoparticles via hydrothermal route utilizing *Prunus cerasifera* leaf extract has been reported for the first time. Synthetic route involved optimization for leaf extract. Doped nanoparticles were characterized for crystalline, optical, compositional, and morphological makeup via X-ray diffraction (XRD), ultraviolet-visible spectroscopy, Fourier transform infrared spectroscopy, and scanning electron microscopy. Direct energy bandgap was calculated through Tauc plot. The incorporation of Ag^{+} into Zn^{2+} sites within ZnO crystal was obtained using leaf extract as a reducing agent. Ag inculcated positional modifications in ZnO structure confirmed via XRD-shifted peaks. Ag:ZnO nanoparticles were found to be an efficient nanophotocatalyst against bromocresol green and bromophenol blue ($R^2 = 0.83$ and 0.95, respectively) in direct solar irradiance. Degradation efficiencies up to 86% and 95% in less than 15 min were achieved. Furthermore, the synthesized doped nanoparticles expressed highly active to active zones of inhibition against nine microbes of pathogenic nature toward human and crops. Doped nanoparticles inhibitory activity was found to exceed standard antibiotic drugs ampicillin and amphotericin B in a standard Kirby-Bauer disc diffusion assay. Creditable photocatalytic and antimicrobial activities of synthesized doped nanoparticles signify their prospects in commercialization into nanophotocatalyst and bactericidal/fungicidal agent at industrial scale.

Keywords: biogenic synthesis; brominated dyes; doping; FTIR; pathogens; *Prunus cerasifera*; SEM; XRD.

***Corresponding author: Khuram Shahzad Ahmad,** Department of Environmental Sciences, Fatima Jinnah Women University, The Mall, 46000 Rawalpindi, Pakistan, e-mail: chemist.phd33@yahoo.com, chemist.phd33@fjwu.edu.pk
Shaan Bibi Jaffri: Department of Environmental Sciences, Fatima Jinnah Women University, The Mall, 46000 Rawalpindi, Pakistan

Abbreviations

DI	deionized water
FDNPs	foliar doped nanoparticles
FTIR	Fourier transform infrared spectroscopy
LEDs	light emitting diodes
NA	nutrient agar
PCLE	*Prunus cerasifera* leaf extract
PDA	potato dextrose agar
ROS	reactive oxygen species
SEM	scanning electron microscope
UV-Vis	UV-Visible spectrophotometer
XRD	X-ray diffraction

1 Introduction

On the basis of commendable size ranges particularly miniature ones, nanoparticle (NP) synthetic modes are occupying a significant dimension of nanotechnology. The evolution in this regard has been particularly rapid. These NPs of desirable shapes and sizes are marked with significant biocidal potential; thus, in contrast to the conventional antibiotics, these NPs are capable of exterminating around 650 cells. NPs have been synthesized through different physical and chemical routes enabling the production of NPs having alleviated sizes; however, these routes possess an inherent damage to the environment, economy, and needs manual effort. In contrary to these physicochemical routes, biological entities, i.e. bacteria, fungi, and plants, can be used as the biofactories [1, 2] for NP synthesis. Plants are heavily utilized for this purpose because of their abundant availability and inexpensiveness and there is no requirement for culture maintenance. Biogenic synthesis has been employed for the synthesis of metallic and metal oxide NPs with an aim to make use of environmental-friendly reducing chemicals. Utilization of plant extracts as a green alternative to reducing and stabilizing agents ensures effectiveness over the highly toxic and energy intensive physicochemical routes [3].

ZnO nanoscale materials in varied morphologies, i.e. NPs, nanoflowers, nanowires, nanorods, and thin films, have been known for their remarkable sensing

and optical cum electrical properties and thus have been employed in biological and gas sensing applications [4]. ZnO, being a wide bandgap semiconductor of 3.37 eV, has been proved as a significant photocatalyst, and it exceeds TiO_2 (3.20 eV bandgap) in the case of hydrospheric remediation. Such higher photocatalysis can be attributed to the generation of reactive oxygen species, capacity to mineralize, and provisioning of multiple reactivity sites [5–8]. Furthermore, ZnO is also advantageous because of economic viability and higher light absorption [5–9]. Addition of Ag in ZnO as a dopant entity acquires the interstitial sites and alternative Zn^{2+} sites [10, 11]. Such an addition is also reported to enhance the photocatalytic potential of ZnO via enhanced separation of charge and alleviation in the recombining capacity of electron hole [12] and has been utilized for a variety of organic pollutants' degradation under ultraviolet (UV) light irradiance [13–15]. Photocatalytic potential improvement of Ag:ZnO can be attributed to the presence of dopant on metallic oxide that gives rise to the charge transfer between the semiconductor ZnO and dopant Ag.

The augmented photoresponse exhibited by the ZnO-based wider bandgap derived products is due to higher intrinsic gains through addition of impurity. For the recompense of n-type conductivity as a result of silver dopant addition, there is a dwindling concentration of donating defects. This in turn plays an important role in enhancing the performance of the Ag-doped ZnO-based devices [15]. Such parameters also enhance the scientific possibility of doped nanomaterials to be used in sensing devices, LEDS, photodetectors, and solar-based devices [16]. Photocatalytic technologies based on incorporation of semiconductors has gained momentum in terms of both application and advancements for environmental remediation of atmospheric and hydrospheric compartments [17]. Doping of different metals on ZnO has been done [10, 18] and found to be playing an influential role in altering the metal oxides' properties [19]. Scientific knowledge regarding the lower dimensional Ag-doped ZnO materials has been scanty. Metals of Ib are found to be exceeding as diffusers in case of semiconductors [10, 16, 18].

Prunus cerasifera is an angiospermic plant belonging to Rosaceae, Prunoideae, and Prunus. This plant is commonly known as Cherry plum and distributed in European and Asian regions. In Pakistan, it is found in Parachinar valley. Fruits of *P. cerasifera* are particularly famous because of characteristic sweet sour flavor, and it is being utilized in making wine, jams, and marmalades in addition to its use as a remedy for jaundice. This rich resource has not been employed for its biological functions on a greater scale neither does it find a higher utilization rate. *Prunus cerasifera* leaves and branches are known for higher quantities of phenols and tannins with an elevated antioxidant action. This plant possesses agronomical significance because it emits various kinds of volatiles, i.e. (*E*)-3-hexen-1-ol, *n*-hexanol and *n*-hexanol, (*Z*)-3-hexenyl butyrate, and (*E*)-2-hexenyl butyrate benzaldehyde [20] from different organs that play a role in defense and relationships with surrounding plant community [21]. The current era dominated by urbanization has adopted various nonsustainable patterns triggering environmental degradation. Such patterns involve indiscriminate synthesis of materials and their reckless dumping into water bodies; e.g. textile industries are known for consuming highest dye levels up to 60%. Of the waste dye, 15% drains off to water in unmodified form [22]. Dyes are persistent in nature because of ringed structure, which is not easily degraded by UV/photoactivation mechanisms, thus posing higher toxicity levels. Thus, the photocatalytic potential of ZnO can further be enhanced via doping to combat this issue [23]. In addition to the vulnerability toward persistent pollutants, the planet Earth and its inhabitants are faced with serious issues of pathogenicity caused by various human and agricultural pathogens. The problem is aggravated when these pathogens exhibit multidrug resistance. There is a need to develop miniature materials that not only can be effective toward resistant strains but also are good in terms of the environment. Furthermore, engineered nanomaterials can be influential in biomedical applications because the occurrence of biological phenomenon including many cellular processes is also at nanoscale. Metallic oxides synthesized via physicochemical routes have been employed for antimicrobial activity [24, 25].

In the present investigation, the strong antioxidant potential and underutilization of *P. cerasifera* leaves has been taken into consideration. The biomimetic synthesis of foliar-mediated silver-doped zinc oxide NPs from *P. cerasifera* leaf extract (PCLE) as a reducing cum stabilizing agent has been reported for the first time by hydrothermal route. Foliar doped NPs (FDNPs) were characterized for different properties via X-ray diffraction (XRD), ultraviolet-visible (UV-Vis) spectroscopy, Fourier transform infrared (FTIR) spectroscopy, and scanning electron microscopy. FDNPs were also assessed for their photocatalytic activity against brominated persistent dyes, i.e. bromocresol green (BG) and bromophenol blue (BB). Moreover, the *in vitro* antimicrobial activity of FDNPs against nine microbes, i.e. *Xanthomonas citri*, *Psuedomonas syringae*, *Aspergillus niger*, *Aspergillus flavus*, *Aspergillus fumigatus*, *Aspergillus terreus*, *Penicillium chrysogenum*, *Fusarium solani*, and *Lasiodiplodia theobromae*, was investigated

by a standard disc diffusion assay in a dose-dependent manner and compared with the standard antibiotics.

2 Materials and methods

Pure silver nitrate (99%; $AgNO_3$), zinc acetate dihydrate ($C_4H_6O_4Zn \cdot 2H_2O$), BG ($C_{21}H_{14}Br_4O_5S$), and BB ($C_{19}H_{10}Br_4O_5S$) were purchased from Sigma Aldrich, St. Louis, MO, USA. Nutrient agar and potato dextrose agar (PDA) culture media were purchased from Merck, Darmstadt, Germany and Liofilchem, Roseto degli Abruzzi, Italy, respectively. All chemicals were of 99% purity and analytical grade and used without further purification. All experiments were done with deionized water (DI). All of the reagents used were purchased from Sigma Aldrich, St. Louis, MO, USA. Devices used in the experimental work were: hotplate (MSH 20D, Wisestir, Germany), centrifuge (C0060-230V, Labnet International, Inc., Edison, NJ, USA), incubator shaker (Irmeco GmbH, Geesthach, Germany), UV-Vis spectrophotometer (1602, Biomedical services, Madrid, Spain), Fourier transformer infra red (8400, Shimadzu, Tokyo, Japan), GCMS (QP5050, Shimadzu, Tokyo, Japan), XRD (Bruker AXS D-8, Shimadzu, Japan), Furnace (550, Ney Vulcan, Bridgeport, CT, USA), SEM (SEMSS-550 Superscan, Shimadzu, Japan), Laminar Flow (Streamline, Singapore), UV lamp (SN500712, Kohler, Hamburg, Germany) and oven (UN110, Memmert, Schwabach, Germany).

2.1 Reducing agent preparation

Healthy and fresh *P. cerasifera* leaves were sampled in May 2017 from Alizai, Parachinar, Pakistan (latitude: 33°53′1.29″N, longitude: 70°6′35.49″E). Leaves were twice tap water washed for removal of possible dust particles and shade dried until complete moisture removal. Leaves were then dried in an oven at 60°C for 30 min for achieving complete dried biomass and then ground to fine powder, sieved, and stored at room temperature. For aqueous extract, 30 g of leaves were dispersed into 30 ml of DI in a 250 ml Erlenmeyer flask at 30°C for 10 min. PCLE was then filtered with Whatman no. 1 filter paper (pore size: 11 µm) and refrigerated at 4°C for further use in synthesis of FDNPs (Figure 1). PCLE, before every experiment, was centrifuged at 4000 rpm to ensure complete mixing of extract.

2.2 FDNPs green synthesis

FDNPs were synthesized via green hydrothermal route. Synthesis was initiated by dissolution of 3.357 g of $C_4H_6O_4Zn \cdot 2H_2O$ (5.08×10^{-7} mol l^{-1}) into 30 ml of DI and 4 g of NaOH (3.33×10^{-6} mol l^{-1}) in 30 ml of DI in a dropwise manner with constant stirring till 30 min, and $Zn(OH)_2$ was formed. It was followed by the transfer of prepared mixture to a Teflon-lined autoclave at 120°C for 20 h. The product was

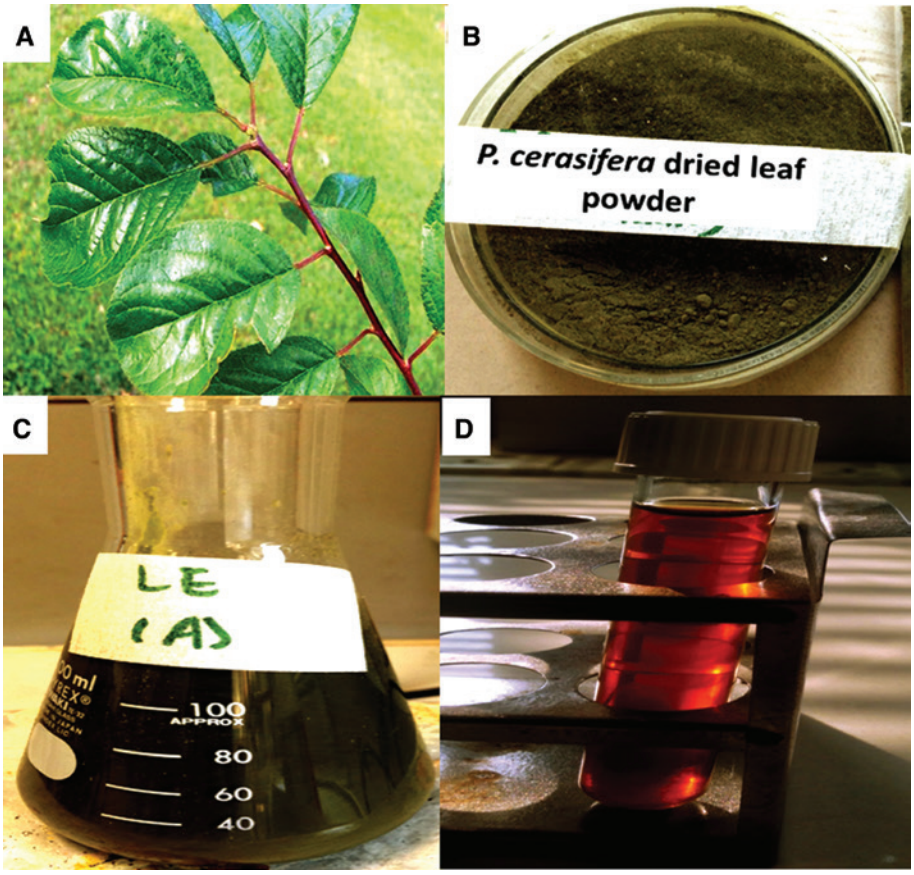

Figure 1: *Prunus cerasifera* leaves: (A) tree, (B) leaf powder, (C) leaf extract in deionized water, and (D) filtered leaf extract used as a reductant in foliar doped nanoparticles synthesis.

then cooled at ambient temperature and centrifuged. DI washing followed by ethanol washing was done for removal of residue, and it was cooled in an oven at 60°C for 12 h. $C_4H_6O_4Zn \cdot 2H_2O$ (5.08×10^{-7} mol l^{-1}) and $AgNO_3$ (1.51×10^{-8} mol l^{-1}) were then dissolved into 30 ml of DI, while 30 ml of PCFE was added dropwise to the mixture with constant magnetic stirring for 15 min. Consequently, precipitates were formed. The mixture was then transferred to Teflon-lined autoclave at 120°C for 20 h. The product obtained after thermal treatment was labeled as Ag:ZnO NPs, and they were centrifuged at 6000 rpm, DI and ethanol washed to obtain a residue-free product, and finally dried at 60°C for 12 h. The final product was stored for characterization and used in applications. The same procedure was repeated with variation of 50, 70, and 90 ml of PCLE to obtain the optimized concentration.

2.3 Characterization

The FDNPs were analyzed for crystalline characteristics by recording XRD patterns with Bruker AXS D-8 powder X-ray diffractometer (Shimadzu, Japan), operated at 40 kV, 20 mA, with CuKα radiation ($\lambda = 1.5406$ Å). Optical evaluation was done by UV-Vis spectrophotometer (1602, Biomedical Services, Spain) in the range of 200–800 nm. For UV-Vis, the FDNP homogenous suspension was prepared by dispersion of FDNPs in DI. The sample was sonicated for 25 min and then analyzed. The FDNPs were analyzed for functional groups using FTIR spectrophotometer (8400, Shimadzu, Japan). The FTIR pellet of FDNPs was prepared by mixing FDNPs and KBr (1:3), and the pellet was pressurized at 5 t with the help of a pellet forming dice. It was then analyzed at room temperature. The FDNP size ranges and surface morphology were checked via scanning electron microscopy (SEM JOEL JSM-6490, Germany) by gold coating on sputter coater and observed.

2.4 FDNP nanophotocatalysis

The nanophotocatalytic efficiency of FDNPs was evaluated by investigating the degradation of BG and BB as target pollutants. BG (250 ml) and BB (30 mg l^{-1}) were kept in direct solar irradiance for 1 h from 12:00 to 1:00 P.M. on a sunny day with an average intensity 68–73 Klux (LT300, Extech, UK). Of the FDNPs, 0.125 g was ultrasonically dispersed into the BG and BB solution (250 ml), and it was magnetically stirred in a quartz beaker for 30 min in the dark to allow the pollutant molecules to be adsorbed on FDNPs and for equilibrium to be established. These mixtures were also kept in direct solar irradiance for the previously mentioned duration. Upon exposure to light, both mixtures exhibited color transformation. Of the sample, 5 ml was taken from both samples at pre-determined time intervals and centrifuged at 6000 rpm for 10 min. Samples were also exposed to UV lamp (SN500712, Kohler, Germany) before UV-Vis analysis recorded between 300 and 700 nm. With an increase in the time interval, the FDNPs added dye solutions expressed discoloration, which was spectrophotometrically determined by recording absorbance values at lambda max, and percent degradation was calculated by the following relationship:

$$\% \text{ Degradation} = (A_i - A_f / A_i) \times 100 \quad (1)$$

where A_i represents the dyes' initial absorbance while A_f is the dyes' final absorbance after addition of FDNPs. Reaction rates were also determined for photocatalytic degradation.

2.5 Antimicrobial assay

FDNPs were assessed for their possible conversion into an effective bactericide and fungicide against nine pathogens, i.e. *X. citri*, *P. syringae*, *A. niger*, *A. flavus*, *A. fumigatus*, *A. terreus*, *P. chrysogenum*, *F. solani*, and *L. theobromae*, by standard Kirby-Bauer disc diffusion assay. In both cases, the zones of inhibition were compared with the standard antibiotic drugs ampicillin and amphotericin B, respectively. Prior to conduction of each antimicrobial assay, Petri plates were autoclaved and stored in an oven to avoid any chance of contamination. Laminar flow hood was also spirit cotton swabbed, and UV was turned on for several minutes before initiation of experiment. FDNPs' stock solution was prepared by suspending FDNPs in methanol to get 100 mg/l. The stock solution was sonicated for 30 min with 7 min repeating cycle, and assays were conducted within 1–2 h of this sonication step. FDNPs were treated on microbes in a dose-dependent manner, i.e. 2, 4, 6, and 10 µl, and the most effective dose was obtained. Antibacterial assay was done by preparation of bacterial culture dilutions and autoclaving to obtain final volumes of 10^5–10^6 CFU/ml. Ampicillin, PCLE, and FDNPs were loaded onto the discs placed on nutrient agar plated containing bacterial laws. These were incubated for 24 h at 37°C in the incubator (Sanyo MR-153, GeminiBV, Netherlands) followed by measurement of zones of inhibition (ZOI) in millimeters after 24 h. Antifungal activity was evaluated with freshly produced fungal mycelia on PDA and incubated at 25 ± 1°C for 5 days. Sterilized filter paper discs loaded with amphotericin B, PCLE, and FDNPs were placed on PDA plates containing fungal strains. Zones of inhibition (mm) were measured after 72 h of incubation and compared with amphotericin B.

The current study does not involve any animal or human-based investigations.

3 Results and discussion

FDNPs were synthesized with Ag as dopant and $C_4H_6O_4Zn \cdot 2H_2O$ as host, and PCLE was used as a reducing cum stabilizing agent for its unique phytoconstituents, e.g. flavonoids, terpenes, tannins, phenols, and other substances of reducing nature. Formation of FDNPs was confirmed by conversion of color from greenish brown to white because of the richness of electron functional groups in leaf extract inducing the synthesis of FDNPs. As FDNPs were synthesized via hydrothermal route, instead of chemical reducing agents, e.g. NaOH and tannic acid meant for precipitating the mixture, the present work has alternatively used PCLE, and no reports are available on the angiospermic plant mediated Ag-doped ZnO NPs. There is a simultaneous nucleation of both the dopant and the host, i.e. Ag and ZnO; however, ZnO has elevated growth rates in comparison to Ag because of variation in heats of formation. Consequently, the hydrothermal green synthetic route enables the formation of Ag NPs on ZnO surface. The antioxidant potential of PCLE is involved in either ion exchange or giving rise to complexation between

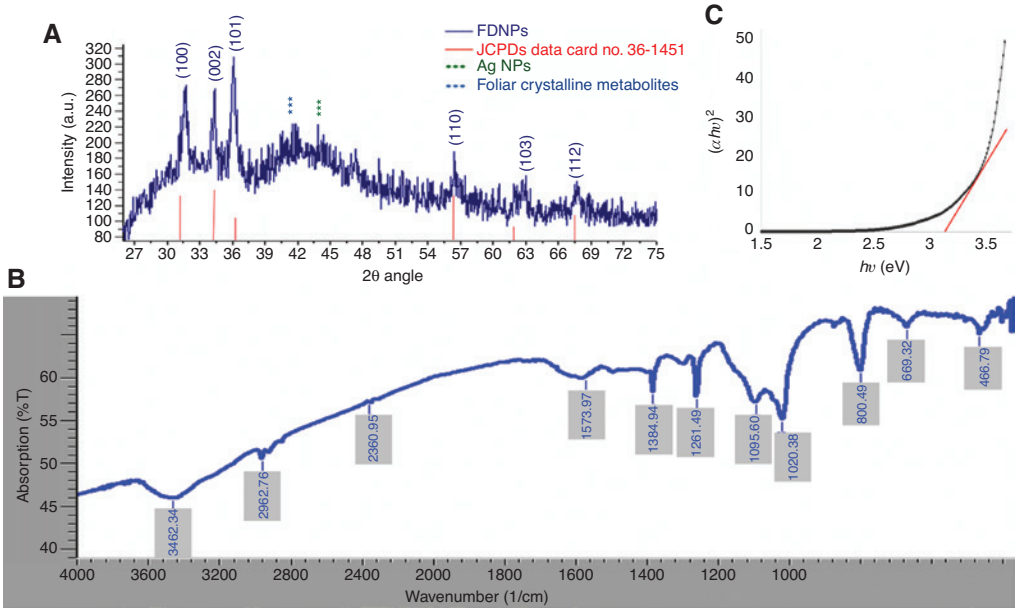

Figure 2: Foliar doped nanoparticles synthesis at highest doped percentage: (A) XRD diffraction spectrum, (B) FTIR spectra, and (C) plot between $h\nu$ (eV) and $(\alpha h\nu)^{1/2}$ for direct bandgap calculation.

metallic ions and polyphenols consequently giving rise to reduction of metallic ions to metallic atoms by extract [26].

XRD pattern of Ag:ZnO NPs has exhibited hexagonal wurtzite geometry of crystals with an average crystallite size of 10.02 nm calculated by Scherrer's equation:

$$D = [K\,\lambda/\beta\cos\theta] \times \text{Å} \tag{2}$$

The diffraction pattern found consistent with the Joint Committee on Powder Diffraction Standards card no. 36-1451 has expressed maximum diffraction from (101) crystal plane. Comparatively, smaller peak at 44.5° corresponds to Ag NP crystal planes, thus confirming the presence of Ag in the tested sample (Figure 2A) [27, 28]. Single Ag NP peak is evident because of smaller quantity and remarkable dispersion rates [29]. Furthermore, current results also confirm the production of Ag NPs and the second phase in the case of synthesis of Ag:ZnO NPs [30]. Ag:ZnO NPs were analyzed for the presence of functional groups by FTIR (Figure 2B and Table 1). The IR band at 3462 cm^{-1} of the O–H stretch corresponding to alcohols and phenols signifies the reducing role of PCLE involved in the synthesis of FDNPs. The IR peaks at 2963, 1574, and 1261 cm^{-1} were assigned to C-H stretch, N-O stretch, and C-N stretch of alkanes, asymmetric stretch of nitro compounds and aromatic amines, respectively [31]. Furthermore, the band at 1020 cm^{-1} is assigned to the in-plane vibrational mode of (NO_3^-) ions. Remarkable doping of Ag:ZnO NPs is expressed in the form of strong vibrational

Table 1: IR peaks for FDNPs synthesized via green hydrothermal route with reducing agents of *P. cerasifera* leaf extract.

FTIR peaks (cm^{-1})	Bond	Functional group
3462	O–H stretch	Alcohols, phenols
2963	C–H stretch	Alkanes
1574	N–O	Asymmetric stretch nitro compounds
1385	C–H rock	Alkanes
1261	C–N stretch	Aromatic amines
1096	C–N stretch	Aliphatic amines
1020	C–N stretch	Aliphatic amines
800	=C–H bend	Alkenes
669	N–H wa	1°, 2° amines

mode. For the calculation of direct energy bandgap of the as synthesized FDNPs, the Tauc plot was used:

$$\alpha h\nu = A(h\nu - E_g)^{1/2} \tag{3}$$

In this equation,
α = absorption coefficient
h = Plank's constant
ν = vibration frequency
E_g = bandgap.

Tauc plot has been obtained by taking $h\nu$ on the horizontal and $(\alpha h\nu)^2$ on the vertical axis. Figure 3C expresses the linear behavior and thus indicative of direct transition of the Ag:ZnO semiconducting NPs. The plot was

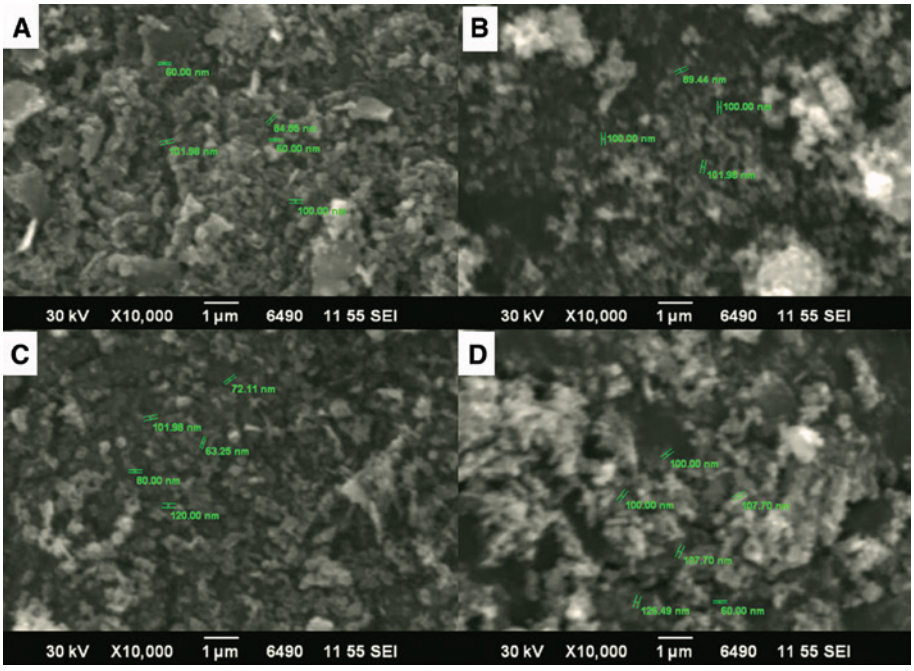

Figure 3: Scanning electron microscopy micrographs of foliar doped nanoparticles at (A) 30, (B) 50, (C) 70, and (D) 90 ml *P. cerasifera* leaf extract concentration.

extrapolated, and the conventional bandgap of ZnO, i.e. 3.37 eV, was found to reduce to 3.1 eV after being doped with Ag, thus expressive of p-type conductivity and revealing its effectiveness in optoelectronics. Achievement of reduction in bandgap ensures the potential of FDNPs as conspicuous candidate for nanophotocatalytic and solar cell based devices. The reduction in bandgap can be attributed to the creation of oxygen vacancy, which augments the electronic transference between valence and conduction bands. Scanning electron microscopy micrographs of FDNPs synthesized with different variations of PCLE are shown in Figure 3. It is quite evident from the micrographs that nanosized particles were obtained at all concentrations of PCLE. Size ranges of 60–101.98, 89.44–101.98, 63.25–120, and 60–126.49 nm were obtained for 30, 50, 70, and 90 ml, respectively. Such ranges signify that 30 and 50 ml is the ideal PLCE concentration for production of FDNPs ≤100 nm, while increasing the concentration beyond this produced FDNPs ≥100 nm. It can be because 30 and 50 ml are the optimum concentrations that can initiate the nucleation of Ag and ZnO in the hydrothermal route.

Human being and aquatic flora and fauna are adversely affected by the textile industry effluents being dumped into water bodies with any processing. Dyes of organic nature are one of the major contributors toward water pollution. Such dyes in most of the cases express higher degrees of recalcitrance and nonbiodegradability. Brominated dyes (Figure 4) in this regard are highly prevalent. Thus, efforts have been done with a variety of materials for remediation of BG [32–36] and BB [32, 37–40] for alleviating the level of harm caused by them to environmental compartments. BG is a brominated dye, which is the most commonly used triphenylmethane dye posing difficulty in breaking down because of the presence of three benzene rings [41]. For BG, photocatalytic and adsorptive processes have been devised to remove it [42, 43], but both of these processes are associated with incurring heavier capital costs and lower efficiencies. BB, also a brominated dye, is one of the most common effluent released from textile and chemical manufacturing plants. It not only interferes with the safety level of water but also affects the aesthetic outlook of water bodies. It is also used as an acid-base indicator and as a color marker for monitoring the process of electrophoretic processes. Excessive

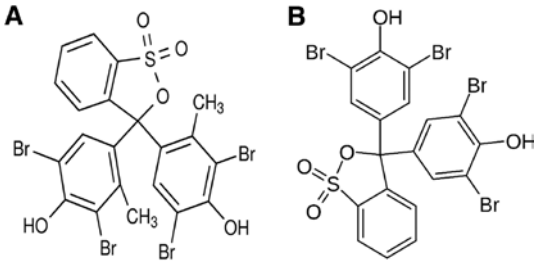

Figure 4: Chemical structures: (A) bromocresol green and (B) bromophenol blue.

Table 2: Time-dependent photocatalytic degradation of the selected brominated dyes with different materials

Dye	Adsorbent	Time of degradation (min)	Reference
BG	Bio-synthesized Au NPs	16	[32]
	ZnO NPs	60	[33]
	Ti/SnO_2-RuO_2 composite	150	[34]
	TiO_2 NPs	180	[35]
	CuO nanowires	210	[36]
BB	Bio-synthesized Au NPs	14	[32]
	Ag^+-doped ZnO NPs	25	[37]
	CuO nano-clinoptilolite	180	[38]
	GO/ZnO nanocomposite	180	[39]
	TiO_2 NPs	240	[40]

BB quantities are known for contamination of lithospheric and hydrospheric compartment because of its profound solubility in water. Thus, remediative technologies have been designed for its removal, e.g. separation mechanisms, precipitative and coagulative processes, oxidation, electrochemical treatment, and adsorptive removal for degradation of organic dyes to benign daughter products [44–47]. Although efforts have been done for the removal of BG and BB with different materials (Table 2), studies involving foliar-mediated Ag:ZnO have never been reported. Thus, current research has attempted to photocatalyze the degradation of BG and BB with green synthesized FDNPs possessing lower bandgap. Upon observation of achromatization (Figure 5) when FDNPs' treated dye solution was exposed to solar radiations, UV-Vis absorption spectra for BB and BG were recorded after every 2 min (Figure 6). Ag:ZnO nanophotocatalyst degraded 86% of BG in 12 min and 95% of BB in 14 min, thus signifying the remediative role of FDNPs (Figure 7).

The natural purification process for BG and BB is extremely slow and inflicts a heavier ecological difference. However, the use of FDNPs ensures quick removal as compared with other materials that have been proved comparatively slower (Table 2). FDNPs upon exposure to direct solar irradiance are marked with formation of charge carriers through light absorption [48–50], thus making FDNPs a unique nanophotocatalyst. Furthermore, the reaction kinetics for FDNPs was determined by plotting $\ln(A_t/A_0)$ vs. time (Figure 7). Photocatalytic degradation processes for both dyes, i.e. BG and BB, exhibited pseudo first-order kinetics with $R^2 = 0.83$ and 0.95, respectively. FDNPs have exhibited a fast and an effective photocatalytic response toward both dyes because of surface plasmonic resonance when they were exposed to light; however, the exact mechanism of photolytic or dye-sensitized mechanism cannot be ruled out. FDNPs in contact with dye solutions are photoactivated because of incoming light, and there is an adherence between the FDNP surface and dye molecules. Consequently, the photoactivation of FDNPs by incoming light also influences and causes excitation of these dye molecules, which releases electron from the lowest unoccupied molecular orbital into the conduction band of semiconductor nanophotocatalyst. This process initiates the delivery of electrons to Ag NPs. Such an electronic transfer generates free radicals known as reactive oxygen species. Reactive oxygen species are remarkably strong oxidants and decompose the brominated dyes [51–54]. Moreover, there is a promotion in the absorptivity of incident light and degradability

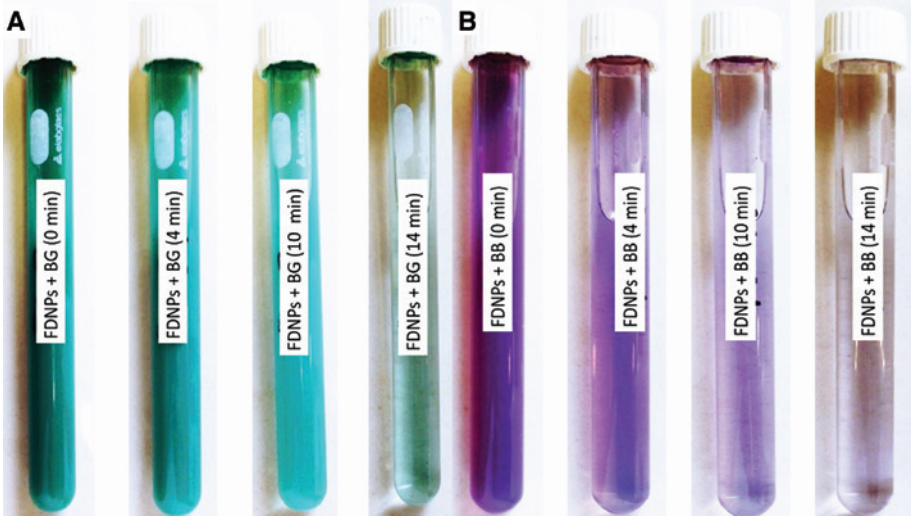

Figure 5: Foliar doped nanoparticles triggered achromatization in (A) bromocresol green and (B) bromophenol blue upon direct solar irradiation.

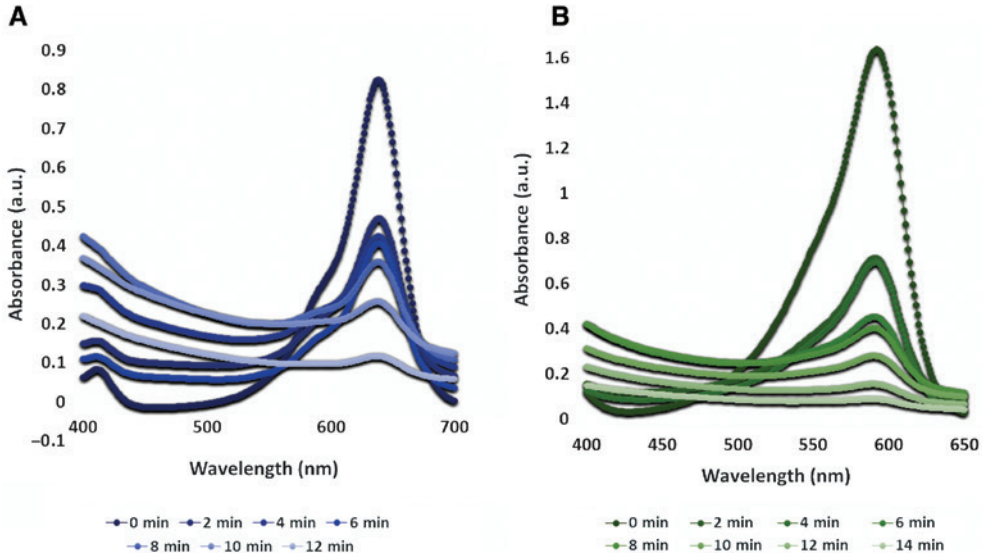

Figure 6: Photocatalytic role of foliar doped nanoparticles and alleviating UV-Vis spectra with time: (A) bromocresol green and (B) bromophenol blue.

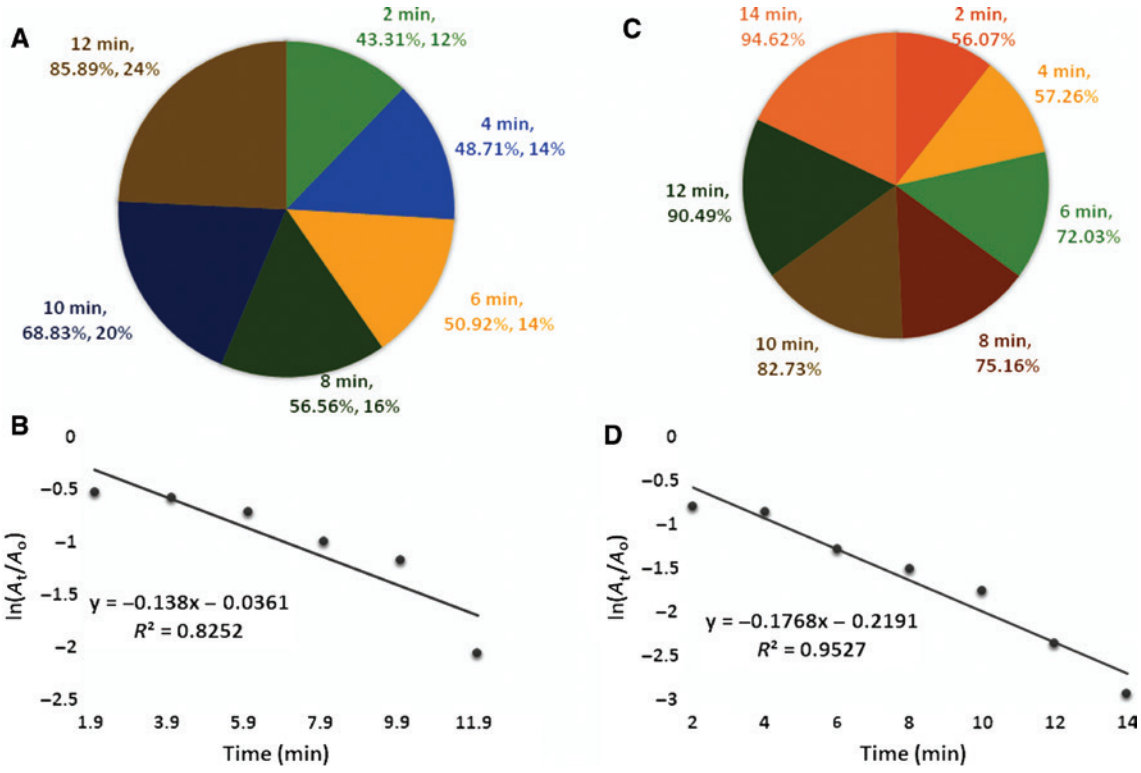

Figure 7: Photocatalytic degradation percentages and reaction kinetics: (A, C) bromocresol green and (B, D) bromophenol blue.

of BG and BB into CO_2 and H_2O due to oxygen vacancies acting as impurity states [55]. Thus, it is evident that the photocatalytic degradation of BG and BB can be a cumulative effect of surface plasmonic resonance, photocatalysis, and photosensitization.

Heavier capital costs spent on antibiotic drugs on an annual basis have not only triggered the financial concerns but also have been proved useless because of the development of resistance in microbes. Thus, a large variety of microbes harmful toward human as well as

agricultural crops is becoming stronger with passage of time. There is a need for the development of antimicrobial agents that not only kill those microbes but also are good in terms of environmental toxicity, cost benefit consideration, and drug resistance. Bacterial and fungal pathogens, i.e. *X. citri*, *P. syringae*, *A. niger*, *A. flavus*, *A. fumigatus*, *A. terreus*, *P. chrysogenum*, *F. solani*, and *L. theobromae*, are known for their higher toxicity rates and have been treated with a variety of antibiotic drugs but are found resistant. However, no studies have been reported on the inhibition of these microbes with foliar-mediated Ag:ZnO NPs. Therefore, the present study has attempted to inhibit the growth of these pathogenic microbes.

In the clinical field, antibacterial agents are of particular significance because these bactericidal agents are associated with fast and improved recovery from bacterial-induced infections and thus play a role in the minimization of drug resistance to some extent. Results confirmed that FDNPs were found effective against all tested microbes (Figure 8). FDNPs produced highly active zones of inhibition against all microbes up to 23.07 mm for *X. citri* followed by 22.02 mm for *A. flavus*. FDNP-induced zones of inhibition against *A. terreus* and *L. theobromae* were comparatively active up to 14.05 and 17.05 mm, respectively. Inhibitory mechanism incurred by metallic NPs is still to be investigated; however, FDNPs are expected to inhibit the bacterial growth either by production of reactive oxygen species on FDNP surface and generation of oxidative stress or by means of toxicity of free metallic ions when they are dissolved [56]. Ag component of FDNPs is known for the production of pits and gaps and ultimate fragmentation of cell of pathogenic microbes.

FDNP-induced lytic mechanism is associated with the interaction of Ag ions with enzymatic disulfide or sulfhydryl groups and consequently annihilating the metabolic processes and cell death. In addition to Ag ions, the ZnO component of FDNPs is also known for its bactericidal activity against a variety of Gram-positive and Gram-negative bacteria in addition to its spores [57, 58]. Bacterial sustainability is affected by FDNPs through production of H_2O_2. Another governing factor in this regard is the agglomeration of FDNPs on bacterial surface due to the generation of electrostatic forces [59]. Bacterial cellular damage is also influenced by cellular membrane disruption and FDNP internalization. Earlier reports have supported the role of Ag and Zn in interrupting the transmembrane electronic transportation [60–62]. When zones of inhibitions were compared with standard antibiotic drugs, FDNPs were found to exceed the efficiency in the cases of *X. citri*, *P. syringae*, *A. niger*, and *A. flavus* for producing higher zones of inhibitions than that of standard bactericidal and fungicidal agent. However, the zones of inhibitions produced against *A. flavus*, *A. terreus*, and *L. theobromae* were comparable with standard antibiotic drugs but did not exceed. FDNP-induced inhibition of *P. syringae* is comparable with chemically synthesized Ag:ZnO NPs [63], and it can be attributed to the provisioning of larger surface area of FDNPs toward microbial contact. Studies have supported the effectiveness of combining NPs with antibiotic drugs, and their synergistic effects were commendable [64]. FDNP-driven antibacterial and antifungal activity was found to be enhancing as the FDNP dose was increased from 2 to 10 µl and was found highest for the highest dose; this finding is consistent with previous

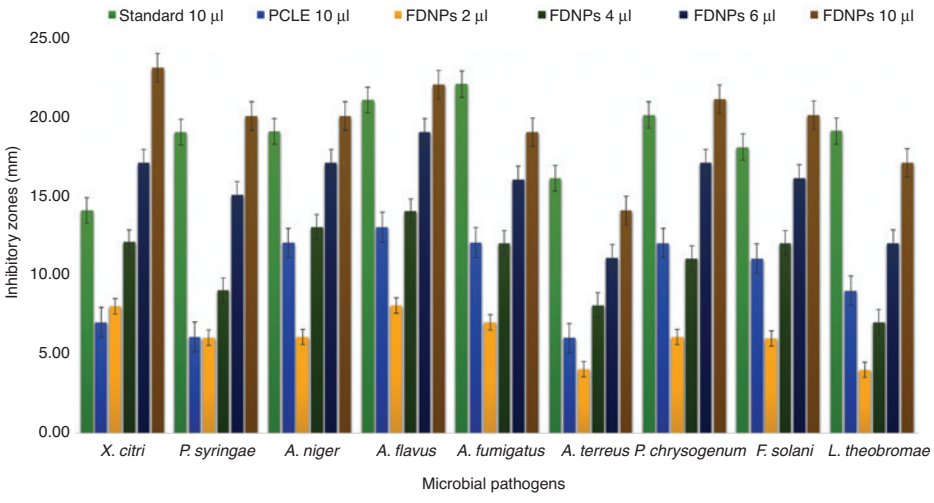

Figure 8: *In vitro* biocidal activity of foliar doped nanoparticles against pathogenic strains exhibiting multidrug resistance (standard for bacterial strains ampicillin and standard for fungal strains amphotericin B).

studies [65–67]. A remarkable inhibitory activity of FDNPs against *X. citri* is significant because this pathogenic strain is responsible for citrus cancer destroying citriculture on a global scale. Thus, FDNPs have very promising prospects to be developed into commercialized bactericidal products against *X. citri* [68]. FDNPs in addition to its development into bactericidal agent are equally effective as a fungicidal agent because of its enhanced antifungal activity [69]. In addition to bacterial action, even in the case of fungal inhibition, higher activity can be attributed to the fact that FDNPs were synthesized from *P. cerasifera* phytoconstituents, and these phytoconstituents have inherent antimicrobial activity, thus causing an augmentation into the antimicrobial action of FDNPs [70]. Antifungal activity of Ag and ZnO NPs against fungal species including *P. chrysogenum* have been demonstrated in a variety of reports [71–74], but the results of present investigation have confirmed the effectiveness of FDNPs against nine microbes.

4 Conclusion

In conclusion, the reducing agents extracted from PCLE can be used for hydrothermal synthesis of silver-doped zinc oxide NPs. The synthesized NPs exhibited commendable crystalline hexagonal wurtzite structure. Ag doping in ZnO can induce an alleviation into direct energy bandgap signifying p-type conductivity and thus enhancing its photocatalytic potential. Moreover, synthesized NPs can also be used as an eco-friendly remediator of BG and BB in direct solar irradiance yielding ≥86% efficiency in less than 15 min. Foliar-mediated Ag:ZnO NPs are of special consideration for their use as an antimicrobial bullets against nine pathogenic microbes having drug resistance. The present study can be extended to the use of synthesized NPs in exploring the exact mechanism of photocatalysis and antibacterial and antifungal annihilation.

Conflict of interest statement: The authors declare no conflict of interest.

References

[1] Gnanadesigan M, Anand M, Ravikumar S, Maruthupandy M, Vijayakumar V, Selvam S, Dhineshkumar M, Kumaraguru AK. *Asian Pac. J. Trop. Dis.* 2011, 4, 799–803.

[2] Patra JK, Thatoi HN. *Acta Physiol. Plant* 2011, 33, 1051–1061.

[3] Mittal AK, Chisti Y. *Biotech. Adv.* 2013, 31, 346–356.

[4] Li Y, Zhao X, Fan W. *J. Phys. Chem. C* 2011, 115, 3552–3557.

[5] Shao R, Sun L, Tang L, Chen Z. *J. Chem. Eng.* 2013, 217, 185–191.

[6] Misra M, Kapur P, Nayak MK, Singla M. *New J. Chem.* 2014, 38, 4197–4203.

[7] Pawinrat P, Mekasuwandumrong O, Panpranot J. *Catal. Commun.* 2009, 10, 1380–1385.

[8] Ong WL, Natarajan S, Kloostra B, Ho GW. *Nanoscale* 2013, 5, 5568–5575.

[9] Lan S, Liu L, Li R, Leng Z, Gan S. *Ind. Eng. Chem. Res.* 2014, 53, 3131–3139.

[10] Lupan O, Chow L, Ono LK, Cuenya BR, Chai G, Khallaf H, Park S, Schulte A. *J. Phys. Chem. C* 2010, 114, 12401–12408.

[11] Lupan O, Pauporté T, Le Bahers T, Ciofini I, Viana B. *J. Phys. Chem. C* 2011, 115, 14548–14558.

[12] Merga G, Cass LC, Chipman DM, Meisel D. *J. Am. Chem. Soc.* 2008, 130, 7067–7076.

[13] Aguirre ME, Rodríguez HB, San Román E, Feldhoff A, Grela MA. *J. Phys. Chem. C* 2011, 115, 24967–24974.

[14] Zheng Y, Chen C, Zhan Y, Lin X, Zheng Q, Wei K, Zhu J. *J. Phys. Chem. C* 2008, 112, 10773–10777.

[15] Thomas MA, Cui JB. *J. Phys. Chem. Lett.* 2010, 1, 1090–1094.

[16] Lupan O, Cretu V, Postica V, Ahmadi M, Cuenya BR, Chow L, Tiginyanu I, Viana B, Pauporté T, Adelung R. *Sens. Actuators B* 2016, 223, 893–903.

[17] Xiong P, Zhu J, Wang X. *Ind. Eng. Chem. Res.* 2013, 52, 17126–17133.

[18] Pauporté T, Lupan O, Zhang J, Tugsuz T, Ciofini I, Labat F, Viana B. *ACS Appl. Mater. Interfaces* 2015, 7, 11871–11880.

[19] Mendoza-Galvan A, Trejo-Cruz C, Lee J, Bhattacharyya D, Metson J, Evans PJ, Pal U. *J. Appl. Phys.* 2006, 99, 014306.

[20] Song W, Qin ST, Fang FX, Gao ZJ, Liang DD, Liu LL, Tian HT, Yang HB. *Appl. Biochem. Biotechnol.* 2017, 27, 1–2.

[21] Reidel RV, Cioni PL, Pistelli L. *Biochem. Syst. Ecol.* 2017, 75, 10–17.

[22] Fukuhara N, Suzuki K, Takeda K, Nihei Y. *Appl. Surf. Sci.* 2008, 255, 1538–1540.

[23] Hosseini SM, Sarsari IA, Kameli P, Salamati H. *J. Alloys Compd.* 2015, 640, 408–415.

[24] Zeng H, Duan G, Li Y, Yang S, Xu X, Cai W. *Adv. Funct. Mater.* 2010, 20, 561–572.

[25] Prasad R, Rattan G. *Bull. Chem. React. Eng. Catal.* 2010, 5, 7–13.

[26] Türkyılmaz ŞŞ, Güy N, Özacar M. *J. Photochem. Photobiol.* 2017, 341, 39–50.

[27] Binks DJ, Grimes RW. *J. Am. Ceram. Soc.* 1993, 76, 2370–2372.

[28] Saoud K, Alsoubaihi R, Bensalah N, Bora T, Bertino M, Dutta J. *Mater. Res. Bull.* 2015, 63, 134–140.

[29] Patil SS, Mali MG, Tamboli MS, Patil DR, Kulkarni MV, Yoon H, Kim H, Al-Deyab SS, Yoon SS, Kolekar SS, Kale BB. *Catal. Today* 2016, 260, 126–134.

[30] Feng HL, Gao XY, Zhang ZY, Ma JM. *J. Korean Phys. Soc.* 2010, 56, 1176–1179.

[31] Georgekutty R, Seery MK, Pillai SC. *J. Phys. Chem. C* 2008,112, 13563–13570.

[32] Choudhary BC, Paul D, Gupta T, Tetgure SR, Garole VJ, Borse AU, Garole DJ. *J. Environ. Sci.* 2017, 55, 236–246.

[33] Kazeminezhad I, Sadollahkhani A. *J. Mater. Sci. Mater. Electron.* 2016, 27, 4206–4215.

[34] Bai H, He P, Chen J, Liu K, Lei H, Zhang X, Dong F, Li H. *Water Sci. Technol.* 2017, 75, 220–227.
[35] Fassi S, Djebbar K, Sehili T. *J. Mater. Environ. Sci.* 2014, 5, 1093–1098.
[36] Farbod M, Ghaffari NM, Kazeminezhad I. *Ceram. Int.* 2014, 40, 517–521.
[37] Abdel-Khalek AA, Nassar HF, Abdel-Gawad FK, Basem SM, Awad S. *Quantum Matter* 2016, 5, 297–304.
[38] Nezamzadeh-Ejhieh A, Zabihi-Mobarakeh H. *J. Ind. Eng. Chem.* 2014, 20, 1421–1431.
[39] Moorthy SK, Viswanathan C, Ponpandian N. In *Nano Hybrids and Composites*, Kuppusami P, Sasipraba T, Eds., Trans Tech Publications: Switzerland, 2017, Vol. 17, pp. 121–126.
[40] Dhanalakshmi J, Padiyan DP. *Mater. Res. Lett.* 2017, 4, 095020.
[41] Nezamzadeh-Ejhieh A, Moazzeni N. *Ind. Eng. Chem. Res.* 2013, 19, 1433–1442.
[42] Ghaedi M, Khajesharifi H, Yadkuri AH, Roosta M, Sahraei R, Daneshfar A. *Spectrochim. Acta A* 2012, 86, 62–68.
[43] Zarei-Chaleshtori M, Correa V, López N, Ramos M, Edalatpour R, Rondeau N, Chianelli RR. *Catalysts* 2014, 4, 346–355.
[44] Bouanimba N, Zouaghi R, Laid N, Sehili T. *Desalination* 2011, 275, 224–230.
[45] Ameen S, Akhtar MS, Seo HK, Shin HS. *Mater. Lett.* 2013, 100, 261–265.
[46] Cao S, Yeung KL, Yue PL. *Appl. Catal. B* 2006, 68, 99–108.
[47] Cao S, Yeung KL, Kwan JK, To PM, Samuel CT. *Appl. Catal. B* 2009, 86, 127–136.
[48] Chauhan R, Kumar A, Chaudhary RP. *J. Sol.-Gel. Sci. Technol.* 2012, 63, 546–553.
[49] Kochuveedu ST, Jang YH, Kim DH. *Chem. Soc. Rev.* 2013, 42, 8467–8493.
[50] Furube A, Du L, Hara K, Katoh R, Tachiya M. *J. Am. Chem. Soc.* 2007, 129, 14852–14853.
[51] Dong G, Zhao K, Zhang L. *Chem. Commun.* 2012, 48, 6178–6180.
[52] Li H, Shi J, Zhao K, Zhang L. *Nanoscale* 2014, 6, 14168–14173.
[53] Xie Y, Yuan C. *Appl. Catal. B* 2003, 46, 251–259.
[54] Zhang X, Wang Y, Hou F, Li H, Yang Y, Zhang X, Yang Y, Wang Y. *Appl. Surf. Sci.* 2017, 391, 476–483.
[55] Leghari SA, Sajjad S, Zhang J. *RSC Adv.* 2014, 4, 5248–5253.
[56] Besinis A, De Peralta T, Handy RD. *Nanotoxic* 2014, 8, 1–6.
[57] Azam A, Ahmed AS, Oves M, Khan MS, Habib SS, Memic A. *Int. J. Nanomed.* 2012, 7, 6003–6005.
[58] Ingle A, Gade A, Pierrat S, Sonnichsen C, Rai M. *Curr. Nanosci.* 2008, 4, 141–144.
[59] Zhang L, Ding Y, Povey M, York D. *Prog. Nat. Sci.* 2008, 18, 939–944.
[60] Hajipour MJ, Fromm KM, Ashkarran AA, de Aberasturi DJ, de Larramendi IR, Rojo T, Serpooshan V, Parak WJ, Mahmoudi M. *Trends Biotechnol.* 2012, 30, 499–511.
[61] Li LH, Yen MY, Ho CC, Wu P, Wang CC, Maurya PK, Chen PS, Chen W, Hsieh WY, Chen HW. *PloS One* 2013, 8, e64794.
[62] Atkinson A, Winge DR. *Chem. Rev.* 2009, 109, 4708–4721.
[63] Ponnuvelu DV, Suriyaraj SP, Vijayaraghavan T, Selvakumar R, Pullithadathail B. *J. Mater. Sci. Mater. Med.* 2015, 26, 204.
[64] Ibrahim HM. *J. Rad. Res. Appl. Sci.* 2015, 8, 265–275.
[65] Janaki AC, Sailatha E, Gunasekaran S. *Spectrochim. Acta A* 2015, 144, 17–22.
[66] Jaffri SB, Ahmad KS. *Artif. Cells. Nanomed. Biotechnol.* 2017, 1–11.
[67] Jaffri SB, Ahmad KS. *Open Chem.* 2018, 16, 1–7.
[68] Ballottin D, Fulaz S, Cabrini F, Tsukamoto J, Durán N, Alves OL, Tasic L. *Mater. Sci. Eng. C* 2017, 75, 582–589.
[69] Rajeshkumar S, Malarkodi C, Vanaja M, Annadurai G. *J. Mol. Struct.* 2016, 1116, 165–173.
[70] Balakumaran MD, Ramachandran R, Balashanmugam P, Mukeshkumar DJ, Kalaichelvan PT. *Microbiol. Res.* 2016, 182, 8–20.
[71] Chitra K, Annadurai G. *Food Res. Int.* 2013, 20, 59–64.
[72] He L, Liu Y, Mustapha A, Lin M. *Microbiol. Res.* 2011, 166, 207–215.
[73] Dimkpa CO, McLean JE, Britt DW, Anderson AJ. *Biometals* 2013, 26, 913–924.
[74] Swain P, Nayak SK, Sasmal A, Behera T, Barik SK, Swain SK, Mishra SS, Sen AK, Das JK, Jayasankar P. *World J. Microbiol. Biotechnol.* 2014, 30, 2491–2502.